HIGH VOLTAGE GAIN WITH NEURAL NETWORK BASED MPPT BASED ELECTRIC VEHICLE

[1] Ms. Prachi Samarth, [2]Prof. Chetan Bobade
[1] PG Student, [2] Head of Department
[1]Department of Electrical Engineering
[1]G.H. Raisoni University, Amravati, India

Abstract: Fuel cell electric vehicles (FCEV) are becoming more common in the automotive industry as a result of tighter restrictions on carbon emissions and fuel economy. A neural network-based maximum power point tracking (MPPT) controller for a 1.26-kW proton exchange membrane fuel cell (PEMFC) that supplies electric vehicle powertrain through a high voltage-gain dc-dc boost converter is presented in this article. The suggested neural network MPPT controller tracks the PEMFC's maximum PowerPoint using a radial basis function network (RBFN) algorithm. For the propulsion of FCEVs, high switching-frequency and high voltage-gain dc-dc converters are needed. A three-phase high voltage-gain interleaved boost converter is also planned for the FCEV system in order to achieve high voltage gain. The interleaving technique reduces the power semiconductor devices' input current ripple and voltage tension. The fuzzy logic controller in the MATLAB/Simulink platform is compared to the performance review of the FCEV framework with the RBFN-based MPPT controller.

IndexTerms **- Proton Exchange Membrane Fuel Cell, MPPT, RBFN, IBC.**

I. INTRODUCTION

Automobile manufacturers are becoming more interested in Fuel Cell Electric Vehicles as a result of environmental emissions and finite fossil fuel sources (FCEV). The major growth of FCEVs [1], [2] has been aided by rapid advancements in power electronics and fuel cell technology. Clean power generation, high stability, high performance, and low noise [3] are all advantages of fuel cells. Fuel cells are classified as Proton Exchange Membrane Fuel Cells (PEMFC), Alkaline Fuel Cells (AFC), Phosphoric Acid Fuel Cells (PAFC), Solid Oxide Fuel Cells (SOFC), and Molten Carbonate Fuel Cells depending on the form of electrolyte substance (MCFC). Because of their low operating temperature and fast start-up, PEMFCs have dominated the automotive industry [4].

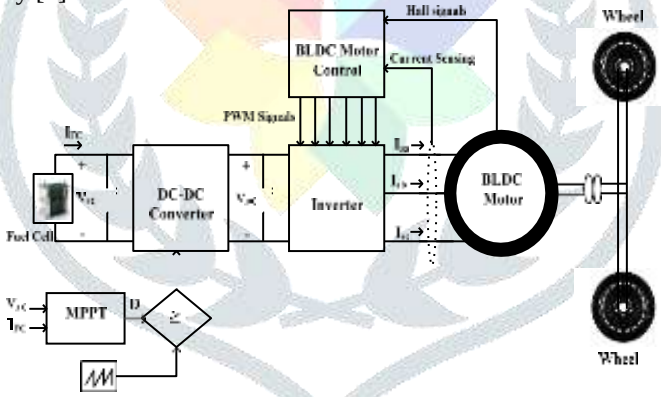

figure1: traditional fuel cell fed BLDC motor driven electric vehicle

The sum of water in the membrane and the temperature of the cell decides the output voltage of the fuel cell. The voltage-current properties of fuel cells are non-linear. As a result, for fuel cells with the highest output voltage and strength, there is only one operation point available. To obtain the most power from the fuel cell at various operating conditions, the maximum power point tracking (MPPT) technique is required. P&O, particle optimization algorithm (PSO), incremental conductance (INC), fuzzy logic control (FLC), sliding mode control, and neural network (NN) to monitor maximum power point (MPP) are some of the MPPT techniques available in the literature [5] – [8].

Among all of these available MPPT algorithms, P&O is simple, popular, and easy to implement. P&O [9] – [11] and gradual conductance methods cause oscillations at a steady-state, lowering the fuel cell system's performance. Fuzzy logic controller and neural network [12] algorithms are used to track the MPP with improved efficiency and accuracy to solve this problem. To track the MPP of the PEMFC, a radial basis function network (RBFN) based MPPT controller is proposed in this paper. Figure 1 illustrates the FCEV's powertrain architecture. The output voltage of a stack of PEMFCs is unchecked and low. To boost and regulate the PEMFC output voltage, a boost or step-up DC-DC converter is necessary. The boost converter is widely used as a fuel cell's front-end power conditioner.

The conventional boost converter is used as a power electronic interface for low-power applications, while the boost converter might not be compatible with high-power applications due to its low current handling capability and thermal management problems [13]. To address these issues, various high voltage gain DC-DC converters have been proposed in the literature. A quadratic boost converter made up of two boost converters is proposed in [14] to achieve high voltage gain.

However, using two boost converters can minimize the system's overall performance. A cascaded 2-phase interleaved DC-DC boost converter. This topology, on the other hand, has low reliability and performance.

A boost converter with a voltage multiplier cell is proposed to achieve high voltage gain, but the voltage gain of a single multiplier cell is insufficient to drive the FCEV powertrain. The isolated converters with coupled inductors or high-frequency transformers to achieve high voltage gain. The transformer turns ratio [15] is balanced to obtain the high voltage gain. However, relative to non-isolated DC-DC converters, these isolated converters are more costly. To achieve low switching stress and high voltage gain, this paper proposes a three-phase non-isolated interleaved boost converter (IBC) for fuel cell applications. The interleaving technique improves the fuel cell's efficiency while still increasing its power output.

The proposed converter's output voltage is fed to an electric motor by an inverter for vehicle propulsion. In FCEVs, the electric motor plays a key role. The cost and complexity of the fuel cell are significantly reduced when the engine is sufficient

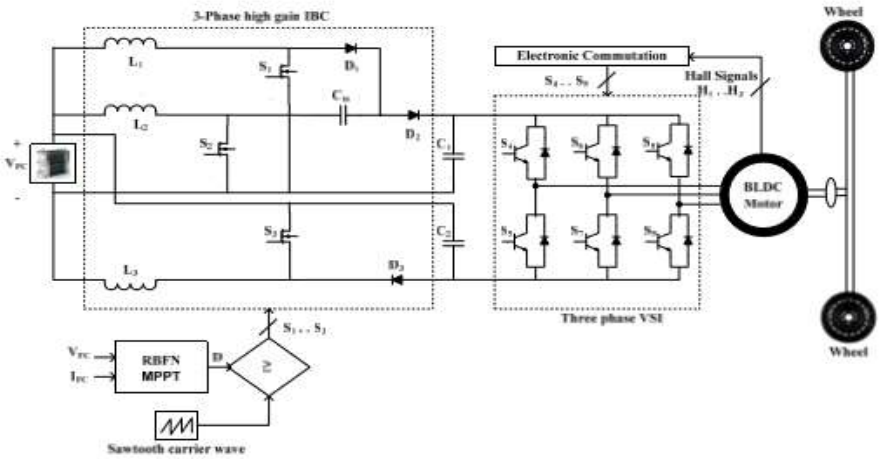

figure2: fuel cell fed BLDC motor driven electric vehicle with proposed RBFN

For electric car applications, the majority of automakers previously used DC motors. Due to the brushes and spinning machines, DC motors, on the other hand, have a high maintenance cost and poor performance [16]. Permanent magnet BLDC motors are currently used mostly in FCEV applications due to their ease of operation, high efficiency, and ruggedness.

The remainder of the article is laid out as follows. section II fuel cell modelling; section III Three-phase high voltage gain IBC; section IV Design of the controller; section V Result analysis and simulation; VI Summaries the findings.

II. FUEL CELL MODELLING

PEM fuel cell is a device that produce electricity through an electrochemical reaction. PEM fuel cell are designed to have good efficiency. An electrochemical system that transforms hydrogen fuel into electricity is known as a fuel cell. Air and gasoline are used as inputs to the fuel cell, and are then converted into water and energy by a chemical reaction. Two electrodes (anode and cathode) and an electrolyte make up a single fuel cell. The electrolyte divides the hydrogen fuel's positive and negative charged ions. In the presence of an electrolyte, electricity is produced at the cell's output as hydrogen and oxygen are fed into it. As a waste product of the chemical reaction, the fuel cell contains only heat and water.

The equation for cell voltage of PEMFC is given as,

$$V_{FC} = E_{Nernst} - V_{act} - V_{ohm} - V_{con} \qquad (2.1)$$

Where, E_{nerest} is reversible (it is open-circuit voltage) thermodynamic voltage.

$$E_{Nernst} = 1.229 - 8.5\times10^{-4}(T - 298.15) + 4.308\times10^{-5}T(\ln(P_{H2}) + 0.5\ln(Po_2)) \qquad (2.2)$$

In equation (2.2), P_{H2} and P_{O2} are hydrogen and oxygen partial pressures (atm) respectively T is the absolute temperature (K).

The chemical reaction formula for a fuel cell is described as

$$2H_2 + O_2 = 2H_2O + energy$$

$$V_{act} = -[\delta_1 + \delta_2 T + \delta_3 T\ln(C_{o2}) + \delta_4 T\ln(I_{FC})] \qquad (2.3)$$

In equation (2.3)

CO2 is called as concentration content of the dissolved oxygen (O2) at the gas or liquid interface and δi (i = 1,2,3,4) is the value of coefficient for each cell

The dissolved oxygen can be given by using the below expression

$$C_{o2} = \frac{P_{o2}}{\left(5.08\times10^{6}\right)\times\exp(-498/T)} \qquad (2.4)$$

Ohmic overvoltage V_{ohm} is expressed as

$$V_{ohm} = I_{FC}(R_c + R_M) \qquad (2.5)$$

R_C term is the resistance of proton. Resistance (RC)is taken as constant.

$$R_M = \frac{\rho_m L}{A} \qquad (2.6)$$

Where, L is membrane thickness (cm), A denotes active area of membrane (cm^2) and ρ_m is the membrane specific resistivity (Ω-cm) and is equation is given as

$$\rho_m = \frac{181.6[1+0.03J+0.062(T/303)^2(J)2.5]}{[G-0.634-3J]\exp[4.18(1-303/T)]} \qquad (2.7)$$

Where G is water content of the membrane and J is current density and is expressed as

$$J = \frac{I_{FC}}{A} \qquad (2.8)$$

Where, R is universal gas constant and J_{max} is maximum current density, F is Faraday's constant.

A DC-DC converter is attached to the output of the fuel cell to maintain a constant voltage across the DC link. The design specifications of 1.26kW PEMFC are given in table below.

Table 1. 1.26 kw PEMFC parameter specification

Parameter Description	Rating
Maximum power (P_{max})	1.26KW
Maximum Current (I_{max})	52 A
Maximum Voltage (V_{max})	24 VDC
Temperature (T)	55^OC
Number of cells	42
Nominal air flow rate	2400

III. THREE-PHASE HIGH VOLTAGE GAIN IBC

Three switches (S_1, S_2, and S_3) and three diodes are used in the suggested converter (D_1, $D_2$and D_3). L_1, L_2, and L_3 are the phase-1, phase-2, and phase-3 filtering inductors, respectively. The input voltage is V_{FC}, the output voltage is V_O, and the load resistor is R. For the study of the proposed high voltage gain IBC, the following assumptions are taken into account:

i. All three phases' inductors are considered to be perfect (L_1=L_2=L_3=L).
ii. The filtering capacitors C1 and C2 are treated as one and the same (C_1=C_2=C).
iii. The suggested converter runs in Continuous Conduction Mode at all times (CCM).
iv. Very modest voltage and current fluctuations are anticipated across the capacitor and the inductor.

Two gate pulses that are 180° phase shifted are used to turn on the switches S_1, S_2, and S_3. Switch S_2 receives one gate pulse, whereas switches S_1 and S_3 get a gate pulse with a 180° phase- shift. Figure 3 depicts the functioning of the proposed converter in various operating modes, whereas Figure 4 depicts the steady-state waveforms of the converter.

Mode 1 (t0≤t≤t1): In this mode, all three switches (S_1, S_2, and S_3) are turned on, and all three diodes (D_1, D_2, and D_3) are reverse biased, as illustrated in Fig. 3(a). The inductors L_1, L_2, and L_3 are charged by the input voltage source V_{FC}. With a slope of (V_{FC}/L), the current through these inductors I_1, I_2, and I3 grew linearly. C_{in} is, the input capacitor, is separated from both the load and the supply. The load resistor receives energy from the output capacitors C_1 and C_2, and the voltage of the output capacitors $V_{C1}$and V_{C2} drops with a slope of (-V_O/RC).

Mode-2 (t1≤t≤t2): The switch S_2 is turned on, while the switches S_1 and S_3 are turned off. As indicated in Fig. 3(b), the diodes D_1 and D_3 are forward biased, whereas the diode D_2 is reverse biased. With a slope of (V_{FC}– V_{Cin})/L and (V_{FC}–V_{C2})/L, the current through the inductors $L_1$and L_3 dropped. With a slope of (V_{FC}/L), the current via the inductor L_2 grows. The input voltage V_{FC} charges the capacitor C_1 which gives energy to the load. The input voltage V_{FC} also charges the capacitors C_2 and C_{in}.

Mode-3 (t3≤t≤t4): Mode 3 is quite similar to mode-1. All three switches (S_1, S_2, and S_3) are turned on, but the three diodes (D_1, D_2, and D_3) are turned off.

Mode-4 (t4≤t≤t5): The switch S_2 is turned off, and the switches S_1 and S_3 are turned on. As illustrated in Fig. 3(c), the diodes D_1 and D_3 are reverse biased, while the diode D_2 is conducting (c). The inductors $L_1$and L_3 are charged by the input voltage source V_{FC}, and the current via these inductors grows with a slope of (V_{FC}/L). With a slope of (V_{FC}+ $V_{C\,in}$ -V_{C1})/L, the current via the inductor L_2 drops. The load receives energy from the capacitors C_2 and C_{in}. The input voltage V_{FC} charges the capacitor C_1.

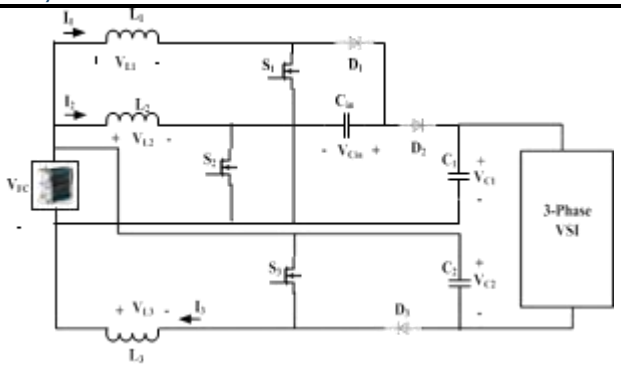

(a)

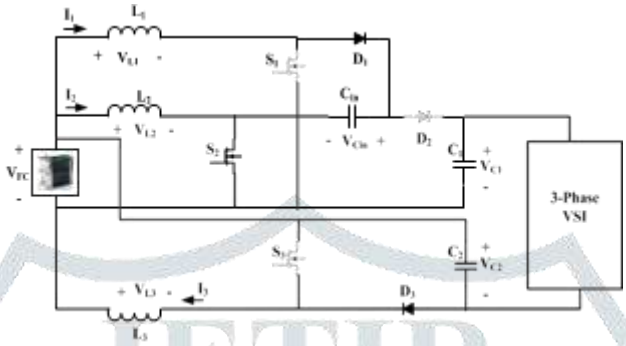

(b)

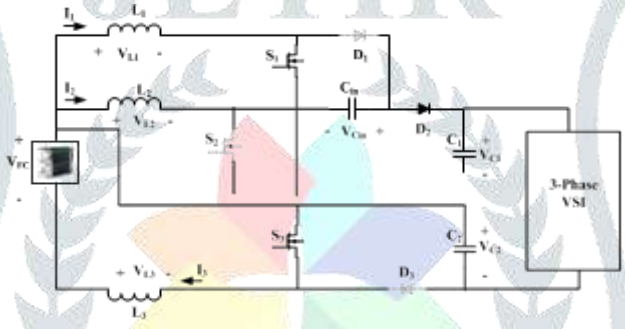

(c)

Figure 3. Operation modes of 3-phase high voltage gain IBC.

A. THE CONVERTER'S ANALYSIS

Inductors, capacitors, and power semiconductor devices are considered to be perfect, and the converter is run in Continuous Conduction Mode (CCM) to simplify the study. The DC-DC converter's static voltage gain (M) is derived by applying volt-second balancing to inductors L_1, L_2, and L_3. We acquire volt-second balance by applying volt-second balance to the inductor L_1.

$$V_{L1} = V_{FC}(t_1 - t_0) + (V_{FC} - V_{Cin})(t_2 - t_1) + V_{FC}(t_3 - t_2) + V_{FC}(t_4 - t_3) = 0 \qquad (3.1)$$

From Eq. (3.1), input capacitor voltage V_{Cin} is obtained as follow

$$V_{Cin} = \frac{V_{FC}}{(1-D)} \qquad (3.2)$$

By applying volt-second balance to the inductor L_2,
we get

$$V_{L2} = V_{FC}(t_1 - t_O) + V_{FC}(t_2 - t_1) + V_{FC}(t_3 - t_2) + (V_{FC} + V_{Cin} - V_{C1})(t_4 - t_3) = 0 \qquad (3.3)$$

Solving Eq. (3.3)

$$V_{C1} = \frac{V_{FC}}{(1-D)} + V_{Cin} \qquad (3.4)$$

From Eq. (3.2) and Eq. (3.4) we get,

$$V_{C1} = \frac{2V_{FC}}{(1-D)} \qquad (3.5)$$

By applying volt-second balance to the inductor L3, we get

$$V_{L3} = V_{FC}(t_1 - t_O) + (V_{FC} - V_{C2})(t_2 - t_1) + V_{FC}(t_3 - t_2) + V_{FC}(t_4 - t_3) = 0 \qquad (3.6)$$

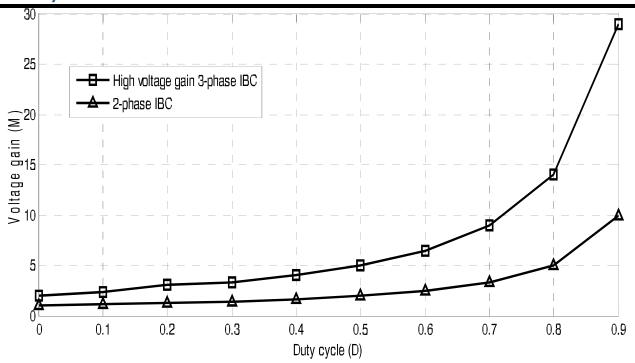

Figure 4. Voltage gain comparison of 3-phase high voltage gain IBC with 2-phase IBC

From Eq. (3.6), capacitor C_2 voltage is obtained as

$$V_{C2} = \frac{V_{FC}}{(1-D)} \qquad (3.7)$$

The output voltage of the converter is obtained by using the Eq. (3.8)

$$V_O = V_{C1} + V_{C2} - V_{FC} \qquad (3.8)$$

From Eq. (14), (16) and (17), the converter static voltage gain M is obtained as

$$M = \frac{V_0}{V_{FC}} = \frac{(2+D)}{(1-D)} \qquad (3.9)$$

The suggested converter's voltage gain is compared to that of a typical two-phase IBC in Fig 4. In mode-2, the switches S_1 and S_3 are turned off, although they stay on in all other modes. The voltage stress of switches S_1 and S_2 may be represented as shown in Fig. 3(b).

$$V_{S1} = V_{Cin} = \frac{V_{FC}}{(1-D)} \qquad (3.10)$$

$$V_{S2} = V_{C1} - V_{Cin} = \frac{V_{FC}}{(1-D)} \qquad (3.11)$$

The switch S_2 is switched OFF in only mode 4. From Fig.3 (c), the voltage stress of switch S_3 is expressed as

$$V_{S3} = V_{C2} = \frac{V_{FC}}{(1-D)} \qquad (3.12)$$

Voltage stress of diode D_1, D_2, D_3 is given by

$$V_{D1} = -V_{C1} = -\frac{2V_{FC}}{(1-D)} \qquad (3.13)$$

$$V_{D2} = V_{Cin} - V_{C2} = -\frac{V_{FC}}{(1-D)} \qquad (3.14)$$

$$V_{D3} = V_{C2} = \frac{V_{FC}}{(1-D)} \qquad (3.15)$$

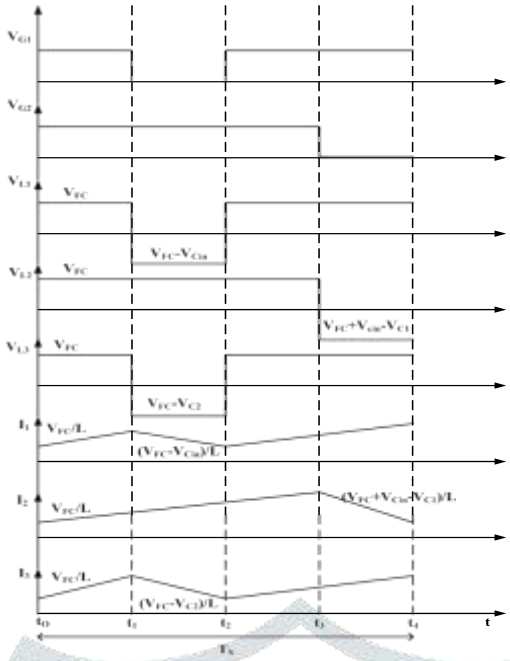

Figure5. Steady-state waveforms of 3-phase high voltage gain IBC

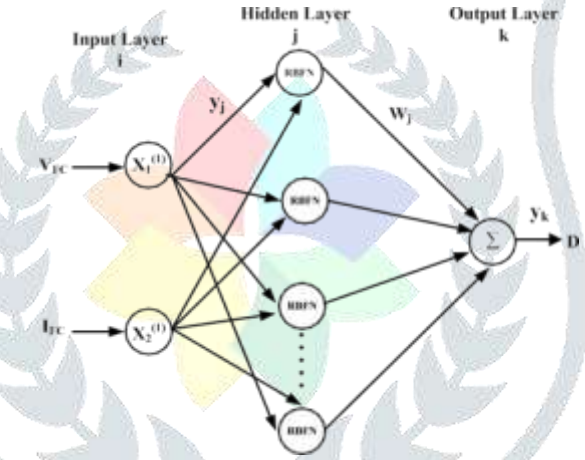

Figure 6. structure of RBFN

The input current ripple is used to construct the inductance L. 20 percent of the input current is believed to be the maximum input current ripple. Using Eq., the value of the input inductor is computed (3.16).

$$L = L_1 = L_2 = L_3 = \frac{DV_{FC}}{\Delta I f s} \qquad (3.16)$$

Similarly, the voltage ripples across the input and output capacitors are used to build the input and output capacitors. One volt of voltage ripple is equal to ten percent of the input voltage.

$$C_{in} = \frac{V_0}{R\Delta C_{\text{in}}\, fs} \qquad (3.17)$$

$$C = C_1 = C_2 = \frac{DV_0}{R\Delta V f s} \qquad (3.18)$$

IV. DESIGN OF THE CONTROLLER

The suggested configuration employs two control techniques. One is for tracking the fuel cell's maximum power, and the other is for BLDC motor operation.

A. MPPT CONTROLLER BASED ON RBFN

It is required for fuel cell systems in order to extract maximum power under various temperature conditions. A RBFN-based MPPT controller is designed for the suggested configuration, and the results are compared to FLC.

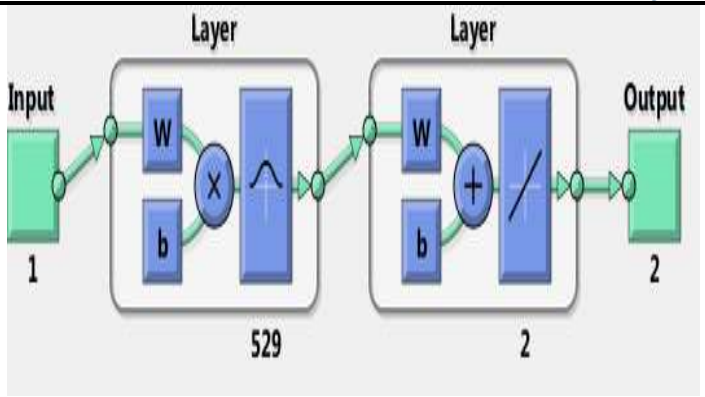

Figure 7. MPPT architecture for the fuel cell based on RBFN

Table 2. Switching states for electronic commutation of BLDC motor

	Hall Signals			Switching States					
Deg	H1	H2	H3	S4	S5	S6	S7	S8	S9
NA	0	0	0	0	0	0	0	0	0
0-60	1	0	1	1	0	0	1	0	0
60-120	1	0	0	1	0	0	0	0	1
120-180	1	1	0	0	0	1	0	0	1
180-240	0	1	0	0	1	1	0	0	0
240-300	0	1	1	0	1	0	0	1	0
300-360	0	0	1	0	0	0	1	1	0
NA	1	1	1	0	0	0	0	0	0

The RBFN is a feed-forward neural network architecture that includes both supervised and unsupervised learning stages. As illustrated in Fig.6, RBFN normally has three layers: an input layer, a hidden layer, and an output layer. The output layer is linear, but the hidden layer uses a non-linear radial basis activation function [16]. The input layer's transport data to the hidden layer[16] The input neuron's net input and output are expressed as

$$X_i^{(1)}(n) = net_i^{(1)} \quad (4.1)$$

$$y_i^{(1)}(n) = f_i^{(1)}[net_i^{(1)}(n)] = net_i^{(1)}(n), i = 1,2 \quad (4.2)$$

Where $X_i^{(1)}$ denotes the input layer, $y_i^{(1)}$ is the hidden layer, and net $_i^{(1)}$ is the sum of the input layers. In the buried layer, every node behaves like a Gaussian function.

In the RBFN, the Gaussian function is utilized as a membership function

$$net_j^{(2)}(n) = -(X - M_j)^T \sum_j (X - M_j) \quad (4.3)$$

$$y_i^{(2)}(n) = f_i^{(2)}[net_j^{(2)}(n)]\exp[net_j^{(2)}(n)], j = 1,2 \quad (4.4)$$

Where M_j and $\sum$j are the Gaussian function's mean and standard deviation, respectively. The linear control signal is generated by the output layer, which contains a single node k. (D)

$$net_k^{(3)} = \sum_j w_j y_j^{(2)} \quad (4.5)$$

$$y_k^{(3)} = f_k^{(3)}[net_k^{(3)}(n)] = net_k^{(3)}(n) \quad (4.6)$$

The connective weight matrix between the output and hidden layer is W_j. The current and voltage of the fuel cell are used as inputs to the RBFN controller in this research, and the output is duty cycle (D), as illustrated in Fig. **7**.

B. ELECTRONIC COMMUNICATION

The BLDC motor electronic commutation is used to generate control signals for the VSI switches .

For each 60-second interval, three hall sensors are employed to create three hall signals based on the motor rotor position. A decoder circuit converts the produced hall signals into switching pulses for the VSI. In Table 2, the VSI switching states are mentioned.

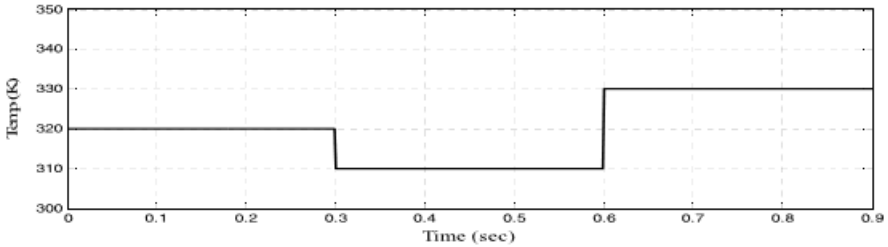

Figure 8. Temperature changes in PEMFC system.

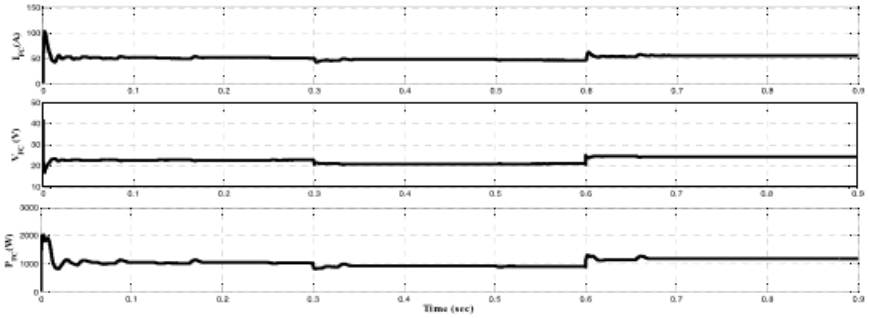

Figure 9. Fuel cell output current, voltage and power at different temperatures

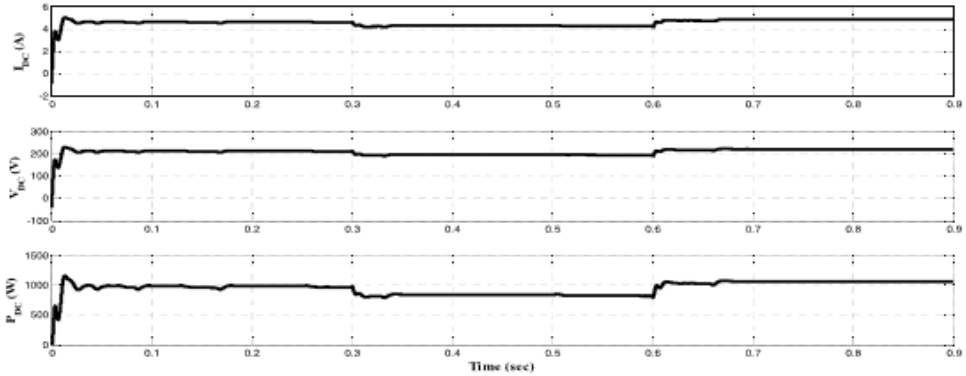

Figure 10. DC link output current, voltage and power at different temperatures using FLC.

V. RESULT ANALYSIS AND SIMULATION

Using the MATLAB/Simulink platform, the performance of the proposed BLDC motor-powered FCEV system is evaluated. Sudden fluctuations in the temperature of the fuel cell are considered for analyzing the dynamic response of the FCEV system, as shown in Fig. 8.

T=320^{o}K for a period of 0 to 0.3sec, T=310^{o}K for a period of 0.3 sec to 0.6 sec, and T=330^{o}K for a period of 0.6sec to 0.9 sec. The output current, voltage, and power waveforms of the fuel cell are illustrated in Fig. 9 for various temperatures.

Fuel cells provide 1080W for 0 to 0.3 seconds, 970W for 0.3 to 0.6 seconds, and 1220W for 0.6 to 0.9 seconds. The dc-link current, voltage, and power are shown in Fig. 10 utilizing the FLC-based MPPT approach. For temperatures of 320k, 310k, and 330^{o}k, it generates 1000W, 830W, and 1150W, respectively. Figure 11 shows the dc link output current, voltage, and power utilizing the proposed RBFN-based MPPT controller. For temperatures of 320^{o}k, 900W, and 330^{o}k, the suggested controller provides 1050W, 900W, and 1200W, respectively. Figure12 shows the performance of the RBFN-based MPPT controller for fuel cells is compared to the performance of the fuzzy logic-based MPPT controller. According to Fig. 12, the suggested controller generates a higher dc link power than the FLC. The comparison table 3 shows the results of the FLC and RBFN controller analyses. The starting and steady-state characteristics of the BLDC motor at various fuel cell temperatures are illustrated in the diagram.

Table 3. Comparison of DC link power with both RBFN and fuzzy controllers

Parameter	**1.26kW PEMFC with fuzzy based MPPT**			**1.26kW PEMFC with fuzzy based MPPT**		
Periods(sec)	0 to 0.3	0.3 to 0.6	0.6 to 0.9	0 to 0.3	0.3 to 0.6	0.6 to 0.9
Fuel cell temperature(K)	320	310	330	320	310	330

DC link current (A)	4.71	4.3	5.1	4.8	4.4	5.21
DC link voltage(V)	212	193	225	220	205	230
DC link power (W)	1000	830	1150	1050	900	1200

Figure 13 shows an example of this. At dynamic temperature settings of the fuel cell, motor parameters such as stator current (Isa), back EMF (E), electromagnetic torque (Te), and load torque (T_L) are shown. 3300 rpm for 0 to 0.3sec, 2400 rpm for 0.3sec to 0.6sec, and 3700 rpm for 0.6sec to o.9sec are the speeds of the BLDC motor. For variable speed circumstances, the torque of the BLDC motor remains constant

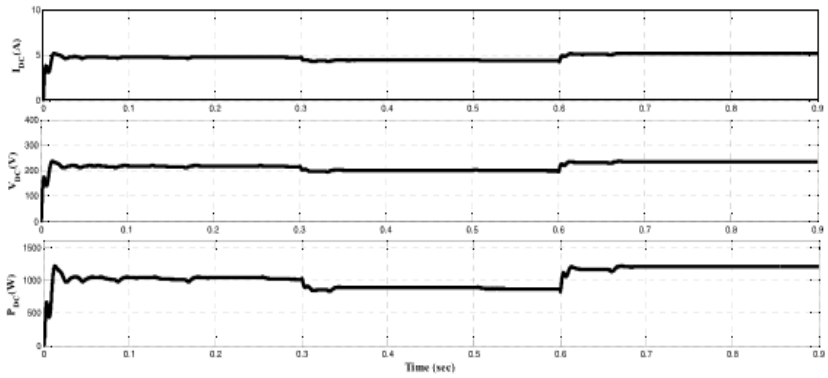

Figure 11. DC link output current, voltage and power at different temperatures using RBFN

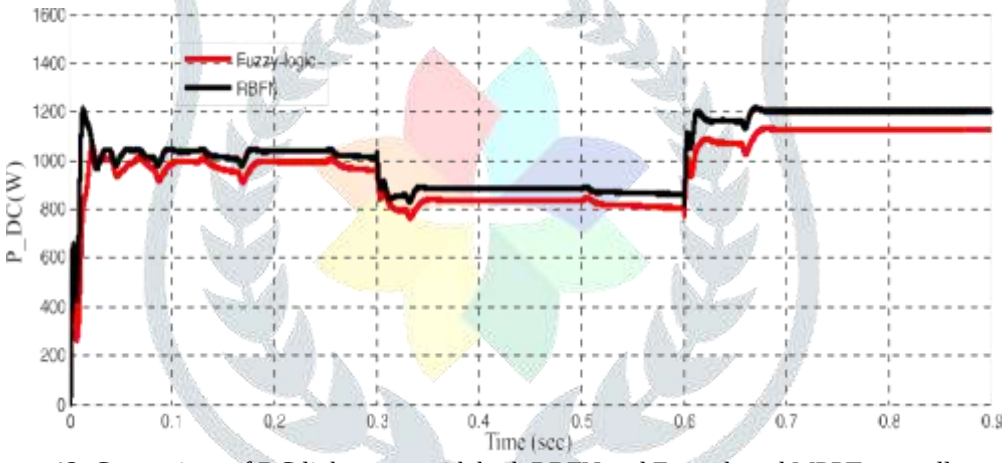

Figure 12. Comparison of DC link power with both RBFN and Fuzzy based MPPT controllers

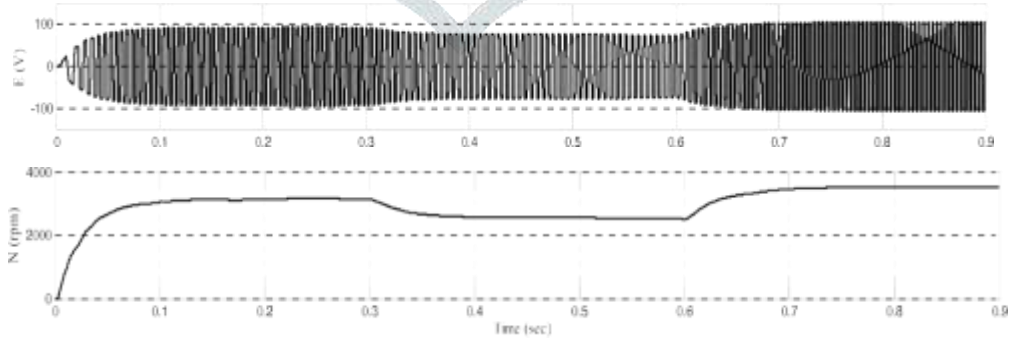

Figure 13. Parameters of BLDC motor

VI. CONCLUSION

A three-phase high voltage gain DC-DC converter is presented for FCEV applications in this study. The suggested converter minimized fuel cell input current ripples as well as voltage stress on power semiconductor switches. For 1.26 kW PEMFC, the RBFN-based MPPT methodology is developed to extract the maximum power from the fuel cell at various temperatures. The FLC MPPT controller is compared to the suggested MPPT methodology. When comparing the RBFN based MPPT controller to the fuzzy logic controller, the simulation results show that the RBFN based MPPT controller has tracked the maximum power point faster. Different performance aspects of the BLDC motor, such as electromagnetic torque, speed, and back EMF, are investigated at various fuel cell system temperatures.

REFERENCES

[1] S. Saravanan and N. R. Babu, ‘‘Maximum power point tracking algorithms for photovoltaic system”—A review Renew Sustain. Energy Rev., vol. 57, pp. 192–204, May 2016.

[2] A. Shahin, M. Hinaje, J.-P. Martin, S. Pierfederici, S. Raël, and B. Davat, ‘‘High voltage ratio DC–DC converter for fuel-cell applications,’’ IEEE Trans. Ind. Electron., vol. 57, no. 12, pp. 3944–3955, Dec. 2010

[3] S. Saravanan and N. R. Babu, ‘‘RBFN based MPPT algorithm for PV system with high step up converter”,Energy Convers. Manage., vol. 122, pp. 239–251, Aug. 2016.

[4] Reddi Rani, Jitendra Gowd, Dharani Lakshmi, “high voltage gain interleaved boost converter with ANFIS based MPPT controller for fuel cell-based applications”, Special Issue, No.-5, January (2020) pp 95-108

[5] H. J. Chiu, L.W. Lin, “A bidirectional DC–DC converter for fuel cell electric vehicle driving system”, IEEE Trans Power Electron., Vol.21(4), pp.950- 958, 2006

[6] N. Mebarki, T. Rekioua, Z. Mokrani, D. Rekioua, S.Bacha, “PEM fuel cell/battery storage system supplying electric vehicle”, Int. J. of Hydrogen Enery., Vol.: 41, Issue: 45, pp.20993-21005, 2016.

[7] Moe Moe Lwin and Htin Lin, “Neural Network Based High-Performance Double Boost DC-DC Converter in Using Renewable Energy System” ,Volume 7, Issue 5, May 2018, ISSN: 2278 -7798

[8] K. Kumar, N. R. Babu, K. R. Prabhu, “Design and Analysis of RBFN-Based Single MPPT Controller for Hybrid Solar and Wind Energy System”, IEEE Access., Vol. 5, pp.15308-15317, 2017.

[9] Mirza Fuad Adnan, Mohammad Abdul Moin Oninda, Mirza Muntasir Nishat, Nafiul Islam, “Design and Simulation of a DC - DC Boost Converter with PID Controller for Enhanced Performance”, IJERT, Vol. 6 Issue 09, September – 2017.

[10] Mehrdad Ahmadi Kamarposhti, Toraj Tayebbifar, Mohammad Shaker, Pegah Nouril, “The Control of Buck Boost DC-DC Converters for DC Motor Drives on variable DC Voltage by Using Neural Network”, Life Science Journal, volume 10, no 5,2013.

[11] Maaspaliza Azri, Nur Hidayah Abu Khanipah “Fuel Cell Emulator with MPPT Technique and Boost Converter “ IJPEDS VOL.8 NO.4 Nov 21, 2017

[12] A. Giustiniani, G. Petrone, G. Spagnuolo, M. Vitelli, “Low current oscillations and maximum power point tracking in grid fuel-cell-based systems”, IEEE Trans Indus Electron., Vol.: 57, Issue: 6, pp. 2042-2053, 2010

[13] L.Egiziano, G.Petrone, G.Spagnuolo, “Optimization of Perturb and Observe Control of Grid Connected PEM Fuel Cells” 25 August 2009

[14] K. Jyotheeswara Reddy, N. Sudhakar,”A new RBFN based MPPT controller for grid-connected PEMFC system with high step-up three-phase IBC” 24 July 2018

[15] B. Geng, J. K. Mills, and D. Sun,”Combined power management/design optimization for a fuel cell/battery plug-in hybrid electric vehicle using multi-objective particle swarm optimization," Int. J. Autom. Technol., vol. 15, no. 4, pp. 645_654, 2014.

[16] B. Singh and R. Kumar, ‘‘Solar photovoltaic array fed water pump driven by brushless DC motor using Landsman converter,’’ IET Renew. Power Generat., vol. 10, no. 4, pp. 474–484, 2016.